Density Waves and Jet Emission Asymmetry in Bose Fireworks

Han Fu, Lei Feng, Brandon M. Anderson, Logan W. Clark, Jiazhong Hu, Jeffery W. Andrade, Cheng Chin, and K. Levin

Phys. Rev. Lett. **121**, 243001 — Published 11 December 2018

DOI: 10.1103/PhysRevLett.121.243001

Density waves and jet emission asymmetry in Bose fireworks

Han Fu,[1] Lei Feng,[1,2] Brandon M. Anderson,[3] Logan W. Clark,[1,2]
Jiazhong Hu,[1,2] Jeffery W. Andrade,[4] Cheng Chin,[1,2] and K. Levin[1]

[1] *James Franck Institute, University of Chicago, Chicago, IL 60637, USA*
[2] *Enrico Fermi Institute and Department of Physics, University of Chicago, Chicago, IL 60637, USA*
[3] *Department of Computer Science, University of Chicago, Chicago, IL 60637, USA*
[4] *Department of Physics, Harvard University, Cambridge, MA 02138, USA*

(Dated: October 30, 2018)

A Bose condensate subject to periodic modulation of the two-body interactions was recently observed to emit matter-wave jets resembling fireworks [Nature 551, 356(2017)]. In this paper, combining experiment with numerical simulation, we demonstrate that these "Bose fireworks" represent a late stage in a complex time evolution of the driven condensate. We identify a "density wave" stage which precedes jet emission and results from interference of matterwaves. The density waves self-organize and self-amplify without breaking the long range translational symmetry. This density wave structure deterministically establishes the template for the subsequent patterns of the emitted jets. Our simulations, in good agreement with experiment, also address the apparent asymmetry in the jet pattern and show it is fully consistent with momentum conservation.

Time-periodic driving, which allows coherent manipulation of many-body systems, is becoming an exciting tool in the field of ultracold atomic gases. Driving provides access to new quantum physics, for example topological states, synthetic gauge fields and Mott transitions [1–7]. Of particular interest is the rather unique capability of these atomic systems to investigate non-equilibrium many-body dynamics [8]. Also unique to ultracold gases is the ability to use Feshbach resonances to periodically modulate atomic interactions [9], as recently implemented by the Chicago group [10, 11] and the Rice group [12–14] on Bose-Einstein condensates. In the Chicago experiment, a collective emission of matter-wave jets resembling fireworks occurs above a threshold modulation amplitude [10].

In the present paper we use the time-dependent Gross-Pitaevskii (GP) equation to study the evolution of the modulated BEC and the emission of jets. We show that the simulations capture well the "Bose fireworks" dynamics seen in experiments. In combination with a new set of experiments, we identify a previously unobserved early stage of the time evolution. Immediately after the onset of modulation, we observe that density waves emerge and grow rapidly within the condensate. The density waves display a high degree of disorder, reflecting quantum fluctuations which we model with a very small [15] random noise term.

As in general parametric resonances [16–20], the density waves set up an effective, self consistently produced "grating" which, through feed-back effects, resonantly amplifies their pattern [21]. (A notable feature distinguishing the parametric resonance here is that the amplification can occur with essentially arbitrary driving frequency.) This process proceeds until pairs of jets (having wavenumber determined by [10, 22] the modulation frequency ω.) are ejected in opposite directions. Within these pair-wise correlations, there remains a quantitative asymmetry that has attracted prior attention [23, 24].

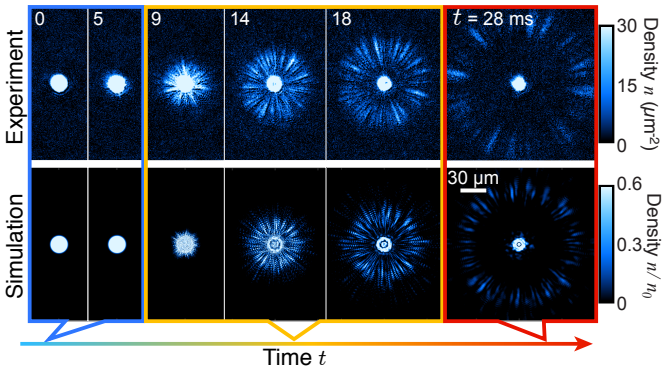

FIG. 1. The real space density distribution $n(\mathbf{r})$ as a comparison between experimental data and simulations. In both, the modulation frequency $\omega/2\pi$ is 2 kHz, the DC and AC interaction energies respectively are $U_0 n_0 \approx h\times 40$ Hz, and $U_1 n_0 \approx h\times 480$ Hz, where h is Planck's constant (see the main text for detailed definitions). As a function of modulation time t, the system exhibits three phases: density waves in a confined condensate (blue box), near-field emission (orange box) and far-field emission (red box).

We focus on two important results: first, we show that the density wave pattern underlies the jet-emission process, and second, we provide a quantitative understanding of the puzzling asymmetry in the emission pattern. Figure 1 summarizes the full evolution of the system and shows good agreement between our simulations and experiment. Three distinct regimes of the Bose fireworks can be identified: the early density wave (DW) regime, the initial emergence of jets (called the "near-field emission") and the well established jet emission regime (called the "far-field emission"). In the near field stage the excited modes begin to leave the condensate while still substantially overlapping with each other. After a sufficiently long time, the matter-wave jets become well separated in the far field and the

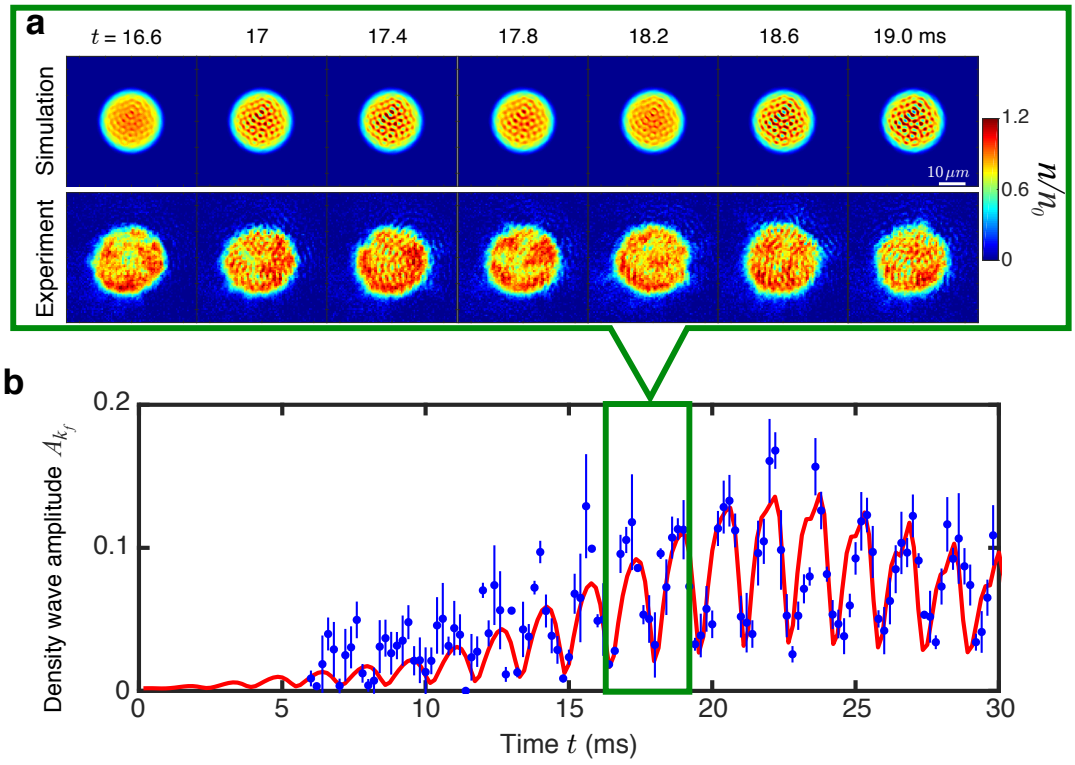

FIG. 2. Experiment and simulation comparison for early-stage density waves (DW) with $|k| = k_f$. (a) The real-space DW oscillations inside the condensate. Theory (top) and experiment (bottom) show good qualitative agreement. The experiment exhibits additional static, long-wavelength density modulations due to trap imperfections. The experimental details are provided in the main text. (b) The amplitude of the density waves in the primary mode comparing simulations (red solid line) and experiments (blue dots with error bars). In addition to fast oscillations, both results show consistent observation of an exponential growth of the envelope until the matter-wave jets are emitted from the condensate.

observed density profiles primarily reflect the populations in momentum-space.

We begin with the theoretical and experimental investigation of the early-stage density waves. Figure 2 presents the experimental observation and theoretical confirmation of the emergence of density waves. The experiments begin with a Bose condensate of 4×10^4 cesium atoms prepared in a uniform disk-shaped trap with a radius of $13\,\mu$m (see Ref. 10 for experimental details). The trap has a potential barrier of height $h \times 200$ Hz in the horizontal direction (h is the Planck constant) and is harmonic vertically with a frequency of 220 Hz. By modulating the magnetic field near a Feshbach resonance, we make the scattering length oscillate as $a(t) = a_{\rm dc} + a_{\rm ac}\sin(\omega t)$ with a small offset $a_{\rm dc} = 4a_0$ and large amplitude $a_{\rm ac} = 40a_0$ at frequency $\omega/2\pi = 620$ Hz, where a_0 is the Bohr radius.

After modulating the interaction for time t, we perform *in situ* imaging and observe density waves forming within the condensate prior to jet emission. Figure 2 (a) shows snapshots of the condensate density distribution $n(\mathbf{r})$ and theoretical simulations. To be more quantitative, we extract the density wave amplitude $A_{k_f} = n_0^{-1}\int_{|\mathbf{k}|=k_f} d\mathbf{k}\,|\tilde{n}(\mathbf{k})|$ from the Fourier transform of the condensate density $\tilde{n}(\mathbf{k}) = (2\pi)^{-1}\int d\mathbf{r} e^{-i\mathbf{k}\cdot\mathbf{r}} n(\mathbf{r})$, see Fig. 2 (b). Here $k_f = \sqrt{m\omega/\hbar}$ is the wavenumber of the density wave determined by the parametric resonance condition; n_0 is the average density of the static condensate prior to interaction oscillations; m is the boson mass; and $\hbar$ is the reduced Planck constant. Interestingly, this density wave amplitude exhibits fast oscillation under a slowly growing envelope.

We note that this density wave pattern is reminiscent of Faraday waves in classical fluids [25, 26] and related to that predicted for driven atomic gases [27–30] as well as observed in a one-dimensional condensate [31]. In contrast to classical Faraday waves our system does not spontaneously exhibit three-fold or higher symmetries. These symmetries are expected to arise from nonlinear kinetic terms in the hydrodynamic equations of motion [25, 26], which are not present in the GP equation.

Our theoretical approach is based on a dynamical GP equation:

$$i\hbar\frac{\partial\psi}{\partial t} = \left[-\frac{\hbar^2}{2m}\nabla^2 + V(\mathbf{r}) + U_0|\psi|^2 - \mu\right]\psi + U_1\sin(\omega t)|\psi|^2\psi, \quad (1)$$

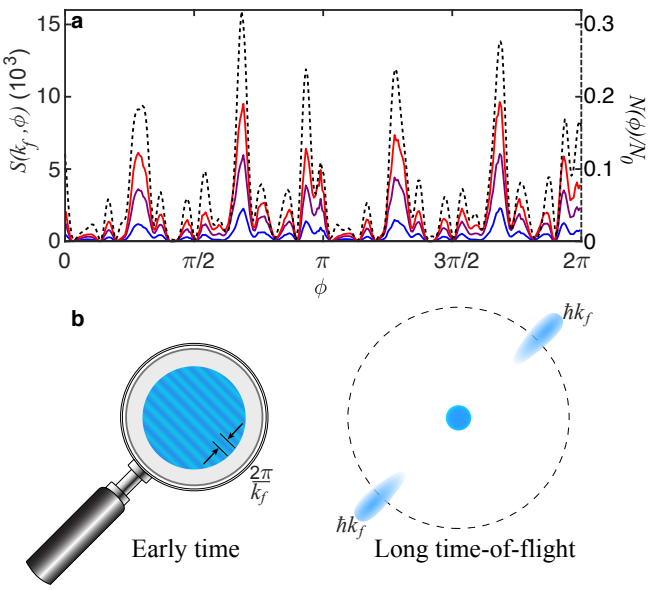

FIG. 3. Connection between density waves before jet emission and the subsequent matter-wave jet pattern. (a) shows the azimuthal density structure factor $S(k_f)$ from a single iteration of the GP simulations at resonant wavenumber k_f at $t = 10$ (blue), 13 (purple), 15 (red) ms prior to jet emission. At each time we observe the same shape with growing amplitude, consistent with the expected amplification process of density waves. The dashed black curve is the real-space azimuthal population distribution of jets $N(\phi)$ at $t = 45$ ms. The scaling factor N_0 is the total number of atoms in the system. The alignment of all maxima and minima between $S(k_f, \phi)$ and $N(\phi)$ shows the equivalence between density waves and jets. (b) schematically shows that the early-time density waves with wavenumber k_f leads to the emission of counter-propagating jets with the same wavenumber k_f at long time.

where ψ is the wavefunction, $\mu = U_0 n_0$ is the chemical potential of the static condensate, $V(\mathbf{r})$ is the external trap potential, and $\mathbf{r} = (x, y)$ is a two-dimensional (2D) spatial coordinate (with origin at the trap center). In addition, $U_0 = 4\pi\hbar^2 a_{\rm dc}/m$ and $U_1 = 4\pi\hbar^2 a_{\rm ac}/m$ are the DC and AC interaction strengths, respectively. At short times, the condensate is weakly excited and the wavefunction can be linearized [27, 28]

$$\psi = \psi_0 \left[1 + \nu(\mathbf{r}, t)\right], \tag{2}$$

where $\psi_0 = \sqrt{n_0} \exp\left[iU_1 n_0 \cos(\omega t)/\hbar\omega\right]$ is the wavefunction of a uniform BEC, and U_0 has been absorbed through the parametrization in Eq. (1). Since the characteristic DW length scales are much smaller than the trap size, we ignore trap effects in our analytical approach. In the plane wave basis we write $\nu(\mathbf{r}, t) = [\xi(t) + i\zeta(t)] \cos(\mathbf{k} \cdot \mathbf{r} + \varphi)$ with both $\xi(t)$ and $\zeta(t)$ real and φ a random phase. Since $|\nu| \ll 1$, ξ satisfies the Mathieu equation for parametric resonances:

$$\frac{\partial^2 \xi}{\partial t^2} + \Omega^2 \left[1 + \alpha \sin(\omega t)\right] \xi = 0, \tag{3}$$

and ζ satisfies the same equation with an extra term $-\alpha\omega \cos(\omega t) \frac{\partial \zeta}{\partial t}$ on the left hand side. Here we keep only leading terms in α; $\Omega^2 = \hbar^2 k^4/4m^2 + U_0 n_0 k^2/m$, and $\alpha = U_1 n_0 k^2/m\Omega^2$.

The solution of Eq. (3) is $\xi(t) \approx A_+ \cos(\omega t/2 + \vartheta_+) \exp(\lambda_+ t) + A_- \sin(\omega t/2 + \vartheta_-) \exp(\lambda_- t)$. Here $A_\pm$ are numerical coefficients, and the exponents are

$$\lambda_\pm = \pm \sqrt{\frac{\alpha^2 \Omega^2}{16} - \left(\Omega - \frac{\omega}{2}\right)^2}. \tag{4}$$

The solution exhibits both subharmonic oscillations with half the driving frequency ω and an exponential envelope growth (via λ_+). For $U_0 \approx 0$ as in experiments, the resonance with maximal λ_+ occurs at $k = k_f$. At this point, $\vartheta_\pm \approx 0$, and $\zeta(t) \approx -A_+ \sin(\omega t/2) \exp(\lambda_+ t) + A_- \cos(\omega t/2) \exp(\lambda_- t)$.

The interference between the uniform background and the excitations then gives the density $n(\mathbf{r}) = n_0|1 + \nu(\mathbf{r}, t)|^2 \approx n_0 \left[1 + 2\xi(t) \cos(\mathbf{k} \cdot \mathbf{r} + \varphi)\right]$, leading to the density waves of exponentially growing envelope that we report here. To provide the full dynamical evolution and to include trap effects, we next appeal to the more complete numerical simulations of the GP equation.

Our simulations are 2D and incorporate a ring trap with inner and outer radii $R_{\rm in}$ and $R_{\rm out}$, respectively. We choose $V(\mathbf{r}) = V_0$ for $R_{\rm in} < r < R_{\rm out}$ and zero elsewhere. V_0 is taken to be compatible with experiment, $R_{\rm in}$ is taken to be the condensate radius, and, as in experiment [10], $R_{\rm out} \approx 1.5 R_{\rm in}$. We use a CUDA-based GP equation solver [32, 33], implemented on graphic processing units, based on a split-step algorithm. At $t > 0$ we introduce a periodic oscillation of the two-body interaction term.

It should be noted that the exponents in Eq. (4) coincide with those derived in Ref. 10 for the matter-wave jets. This suggests that the two forms of excitations may be manifestations of the same physics. We probe this hypothesis in Fig. 3 which contains results from our full GP simulations. Indeed, Fig. 3 provides strong simulation evidence that the density waves are necessary precursors to the jets and that they establish the template for the subsequent jet emission pattern. In particular, we find that the structure factor with fixed extrema (established by the DW pattern at the onset of shaking) is precisely equivalent to the real-space emitted jet population $N(\phi)$ observed after a long propagation time.

The structure factor is defined by $S(k_f, \phi) = N_0^{-1} \int k dk |\tilde{n}(\mathbf{k})|^2$, where the magnitude and phase of the wavevector are $|\mathbf{k}| = k \approx k_f$ and $\phi = \arctan(k_x/k_y)$. Note from Fig. 3 (a) that the structure factor contains random peaks and valleys as determined by the initial random seed which emulates the fluctuations of real experiments. These patterns are established at the onset of shaking, and the only change with increasing time is an exponential growth of the peak amplitudes.

The dashed black line plotted in Fig. 3 (a) is the real-space azimuthal distribution for the jet population $N(\phi) = \int_{\mathbf{r}=(\hbar t/m)\mathbf{k}} r dr\, n(\mathbf{r})$, at long times. Importantly,

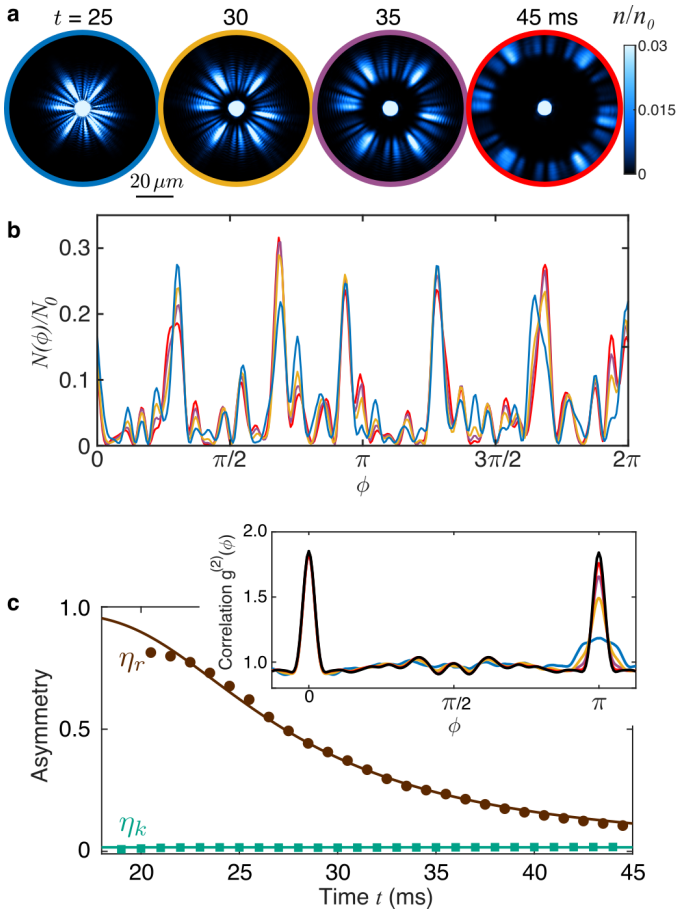

FIG. 4. Time evolution and correlations of the emitted jets. (a) shows the calculated jet emission pattern evolving from the near- to far-field regimes. The calculation is based on identical initial noise seeding. (b) shows the real space azimuthal population of the four images in (a), identified by the same color. Note that the $t = 45$ ms far-field curve is equivalent to that shown dashed in Fig. 3 (a). Here unlike in Fig. 3, the peaks and valleys are slightly displaced with time. Panel (c) probes the emission asymmetry in real space $\eta_r = g^{(2)}(\pi) - g^{(2)}(0)$ (brown circles) and the momentum-space analogue η_k (green squares). The main figure shows that the $(0, \pi)$ asymmetry is always absent in momentum space (η_k is strictly zero within numerical precision) so that momentum is conserved. In real space, using Panel (b) we find that this $(0, \pi)$ asymmetry decreases with increasing time. The inset indicates the correlation function $g^{(2)}(\phi)$ at the same 4 times as in (a), along with an early time momentum correlation function at $t = 20$ ms (black curve). Again, inversion 0-π symmetry is broken at short times, but recovers after long time-of-flight, and is fully preserved in momentum space. The solid line (brown) in (c) is an analytical fit to η_r [34].

the angular distribution shows the equivalence between $S(k_f, \phi)$ and $N(\phi)$. This underlies our claim that density waves and jets are deterministically correlated. These results are summarized in Fig. 3 (b). This presents a schematic plot linking the momentum space spectrum of the DW and the population of jets with the same wavevector $\pm\mathbf{k}$ after long time of flight.

Having established the equivalence between the far-field jets and the initial density waves, one might expect that the same azimuthal distribution would appear in the near-field regime, when jets are first emitted from the condensate. However, our simulations show that this is not the case. In Fig. 4 (a) and (b), a clear modification of the distribution shape with varying time is seen and is accompanied by an "inversion symmetry breaking" (in the near field). This is associated with the observation (reported experimentally [10]) of an asymmetric two-particle correlation function $g^{(2)}(\phi)$ of the jet emission pattern, i.e., $g^{(2)}(\pi) \neq g^{(2)}(0)$.

Here we propose and provide strong numerical support for a scenario which explains this observation and, in contrast to the literature [23, 24], has momentum conservation. This is well substantiated by the detailed numerics summarized in Fig. 4 (c), along with analytical arguments in the supplementary material [34]. To quantify this inversion asymmetry, we introduce a parameter

$$\eta_r = \frac{\left\langle [N(\theta) - N(\theta+\pi)]^2 \right\rangle}{2\left\langle N(\theta)\right\rangle^2} = g^{(2)}(0) - g^{(2)}(\pi)$$

for real space (and its analogue, η_k in momentum space [34]), where $\langle \ldots \rangle$ corresponds to averaging over angles θ and ensembles. Figure 4 (c) plots the asymmetry functions, $\eta_{r,k}$, in real- and momentum-space, together with the corresponding correlation function $g^{(2)}(\phi)$ shown in the inset. The spatial asymmetry η_r decreases from a finite value to zero when going from the near to far field. This indicates that the inversion symmetry is recovered at large times. The momentum-space asymmetry η_k, interestingly, remains zero independent of time, showing clearly that momentum conservation is obeyed at all times.

We attribute this asymmetry to the fact that, in the near field, excitations of different wavevectors substantially overlap with each other. The resulting pattern is derived from interference between these overlapping modes, which have uncorrelated random phases. Thus, when measuring the population at angles θ and $\theta + \pi$, the symmetry between the relevant counter-propagating pair $\pm\mathbf{k}$ ($\tan\theta = k_y/k_x$) is masked by interference from other uncorrelated modes. By contrast, in the far field, different modes are well separated so that each jet now represents a single mode. Here momentum conservation is more apparent and inversion symmetry in real space is recovered [34].

The asymmetry in the emission pattern has alternatively been attributed to di-jet acollinearity due to hydrodynamic collisions, seen, for example, in quark-gluon plasmas [23], or to the Hanbury-Brown-Twiss effect in the angular momentum eigenstate basis within a time-dependent Bogoliubov theory [24]. In this context, our numerical calculations show that momentum conservation persists throughout

the entire evolution, as argued earlier [10]. In this paper we have provided a more intuitive and quantitative picture showing how the asymmetry arises from the interference between overlapping matterwave modes [34].

Conclusions.– The present paper has addressed the jet emission process induced by a periodic drive of the two-body interactions. Through a combination of simulations of the Gross-Pitaevskii equation and experiments, we demonstrated that the jet structure is imprinted in the early stages of an excited condensate, through density waves. Observing the actual density waves in experiments, as reported in the present paper, was key to confirming this picture. Also critical to this analysis is the demonstrated capability of the GP simulations to successfully address experiments involving this stimulated emission over widely varying time, space and momentum coordinates. Our simulations have provided predictive capabilities as well as the ability to establish the important underlying principles (such as momentum conservation) of a broad scope of experimental matter-wave jet observations.

Acknowledgments.

We are grateful to Tom Witten for helpful discussions and Igor Aronson and Andreas Glatz for the numerical GP code. L. F. acknowledges support from an MRSEC-funded Graduate Research Fellowship. L. W. C. was supported by a Grainger Graduate Fellowship. This work was primarily supported by the University of Chicago Materials Research Science and Engineering Center, which is funded by the National Science Foundation under award number DMR-1420709. We also acknowledge support from NSF Grant No. PHY-1511696 and the Army Research Office-Multidisciplinary Research Initiative under grant W911NF-14-1-0003.

[1] A. Eckardt, Rev. Mod. Phys. **89**, 011004 (2017).
[2] G. Jotzu *et al.*, Nature **515**, 237 (2014).
[3] M. Aidelsburger *et al.*, Nature Physics **11**, 162 (2015).
[4] M. Aidelsburger *et al.*, Phys. Rev. Lett. **107**, 255301 (2011).
[5] A. Zenesini, H. Lignier, D. Ciampini, O. Morsch, and E. Arimondo, Phys. Rev. Lett. **102**, 100403 (2009).
[6] J. Dalibard, F. Gerbier, G. Juzeliūnas, and P. Öhberg, Rev. Mod. Phys. **83**, 1523 (2011).
[7] E. J. Mueller, Phys. Rev. A **70**, 041603 (2004).
[8] A. Polkovnikov, K. Sengupta, A. Silva, and M. Vengalattore, Rev. Mod. Phys. **83**, 863 (2011).
[9] C. Chin, R. Grimm, P. Julienne, and E. Tiesinga, Rev. Mod. Phys. **82**, 1225 (2010).
[10] L. W. Clark, A. Gaj, L. Feng, and C. Chin, Nature **551**, 356 (2017).
[11] L. W. Clark, B. M. Anderson, L. Feng, A. Gaj, K. Levin, and C. Chin, Phys. Rev. Lett. **121**, 030402 (2018).
[12] S. E. Pollack, D. Dries, M. Junker, Y. P. Chen, T. A. Corcovilos, and R. G. Hulet, Phys. Rev. Lett. **102**, 090402 (2009).
[13] S. E. Pollack, D. Dries, R. G. Hulet, K. M. F. Magalhães, E. A. L. Henn, E. R. F. Ramos, M. A. Caracanhas, and V. S. Bagnato, Phys. Rev. A **81**, 053627 (2010).
[14] M. C. Tsatsos, J. H. V. Nguyen, A. U. J. Lode, G. D. Telles, D. Luo, V. S. Bagnato, and R. G. Hulet, ArXiv e-prints (2017), arXiv:1707.04055.
[15] The fluctuation term $\psi_s = \varepsilon_r + i\varepsilon_i$ is added to the initial ground state wave function ψ_0. Here we chose the random variables ε_r and ε_i to have a Gaussian probability density function centered around zero with standard deviation $\sigma = 0.1|\psi_0|$.
[16] S. Lellouch, M. Bukov, E. Demler, and N. Goldman, Phys. Rev. X **7**, 021015 (2017).
[17] M. Krämer, C. Tozzo, and F. Dalfovo, Phys. Rev. A **71**, 061602 (2005).
[18] G. K. Campbell, J. Mun, M. Boyd, E. W. Streed, W. Ketterle, and D. E. Pritchard, Phys. Rev. Lett. **96**, 020406 (2006).
[19] N. Gemelke, E. Sarajlic, Y. Bidel, S. Hong, and S. Chu, Phys. Rev. Lett. **95**, 170404 (2005).
[20] L. Fallani, L. De Sarlo, J. E. Lye, M. Modugno, R. Saers, C. Fort, and M. Inguscio, Phys. Rev. Lett. **93**, 140406 (2004).
[21] S. Inouye, A. P. Chikkatur, D. M. Stamper-Kurn, J. Stenger, D. E. Pritchard, and W. Ketterle, Science **285**, 571 (1999).
[22] L. Feng, J. Hu, L. W. Clark, and C. Chin, ArXiv e-prints (2018), arXiv:1803.01786.
[23] M. Arratia, ArXiv e-prints (2018), arXiv:1801.05515.
[24] Z. Wu and H. Zhai, ArXiv e-prints (2018), arXiv:1804.08251.
[25] S. T. Milner, Journal of Fluid Mechanics **225**, 81 (1991).
[26] W. Zhang and J. Viñals, Journal of Fluid Mechanics **336**, 301 (1997).
[27] K. Staliunas, S. Longhi, and G. J. de Valcárcel, Phys. Rev. Lett. **89**, 210406 (2002).
[28] Y. Kagan and L. Manakova, Physics Letters A **361**, 401 (2007).
[29] A. I. Nicolin, R. Carretero-González, and P. G. Kevrekidis, Phys. Rev. A **76**, 063609 (2007).
[30] A. Balaž, R. Paun, A. I. Nicolin, S. Balasubramanian, and R. Ramaswamy, Phys. Rev. A **89**, 023609 (2014).
[31] P. Engels, C. Atherton, and M. A. Hoefer, Phys. Rev. Lett. **98**, 095301 (2007).
[32] P. Scherpelz, K. Padavić, A. Rançon, A. Glatz, I. S. Aranson, and K. Levin, Phys. Rev. Lett. **113**, 125301 (2014).
[33] B. M. Anderson, L. W. Clark, J. Crawford, A. Glatz, I. S. Aranson, P. Scherpelz, L. Feng, C. Chin, and K. Levin, Phys. Rev. Lett. **118**, 220401 (2017).
[34] See Supplement.